IRON OXIDE NANOPARTICLES IN DRUG DELIVERY SYSTEMS

ABEL M.MAHARRAMOV, IRADA N. ALIEVA, GULTEKIN D.ABBASOVA,
M. A. RAMAZANOV[*], NAQIF S.NABIYEV, MOHAMMAD
R.SABOKTAKIN[a]
Baku State University, Z.Khalilov str.23, AZ-1148, Baku, Azerbaijan
[a]International Research Institute of Arian Chemie Gostar, Tabriz, Iran

The geometry and electronic structure of iron oxide Fe_3O_4 with di-glucose and pentapeptide CREKA complex compound have been studied by the semiempirical molecular mechanics MM^+ and quantum chemistry PM3 methods. The geometrical and energy parameters, characterizing the low energy states of the complex, were calculated using the HyperChem 8.03 program. A synthetic macromolecule, aminodextran-coated iron oxide nanoparticles conjugated with CREKA peptide, was then synthesized as a nanocarrier, which was detectable using magnetic resonance imaging. The synthesis process began with a two-step reaction that attached a high density of amino groups to a dextran backbone. The aminodextran–coated iron oxide nanoparticles thus synthesized were characterized using Fourier transform infrared spectroscopy. Also, the morphology of this synthetic macromolecule was studied by scanning electron microscopy.

1. Introduction

The structure and properties of ferromagnetic materials currently attract a great deal of attention. The most widely studied are the iron oxide nanoparticles – magnetite γ-Fe_2O_3 and magnetic Fe_3O_4 [1]. Metal nanoparticles based on iron are prospective materials for use as information carriers, drug delivery systems, etc. Iron has the valuable abilities to reduce and oxidize, to form complex compounds with different biochemical properties, and to participate in electron transmission reactions [2]. Elementary or metallic iron Fe^0 oxidizes to Fe^{3+} in the presence of oxygen and humidity, forming insoluble Fe_2O_3 [3]. Bivalent iron FeO is an intermediate product of iron and ferrites production, and it is a constituent of ceramics and heat resistant enamels. Iron oxide Fe_3O_4 – the tetroxide of trivalent iron (magnetite mineral) ($FeO \cdot Fe_2O_3$ or $Fe^{II}(Fe^{III}O_2)_2$) – when heated in air oxidizes to Fe_2O_3. It is ferromagnetic, has high electroconductivity and dissolves in acids to form Fe^{2+} and Fe^{3+} salts [4,5]. The iron-ligand bonds in such complexes are coordination bonds; the donor-atoms of the ligands give their unbonded electron pairs to the central atom of metal. The bond length of Fe^{III}-O, as determined in various complexes, is 2.10Å at S=5/2 and 1.99Å at S=1/2; the bond length of Fe^{III}–N is 2.32Å at S=5/2 and 1.98Å at S=1/2; the bond length of Fe^{III}–C is 2,31Å at S=5/2 and 1.98Å at S=1/2.

There are a lot of investigations in the literature devoted to the description of super magnetic iron oxide nanoparticles being applied in clinic and diagnostic medicine due to their satisfactory biocompatibility as contrasting agents in magnetic resonance analysis [6,7]. Loaded by thousands of molecules of medicine, the nanoparticles can transport medicine to the exact location of affected tissues [8]. At the same time neither the drugs being transported nor any other components of the complex influence the magnetic properties of the iron oxide nanoparticles.

_____
[*] Corresponding author: nanomaterials@bsu.az, mamed_r50@mail.ru

Despite the impressive success of modern nanomedicine in creating this new class of medications, there is still a lack of complete theoretical models describing the electron structure of the complex compounds of iron oxide nanoparticles with medical molecules [9].

The present study considers the spatial and electron structure of iron (II) and iron (III) oxides in a complex compound of Fe_3O_4 with bi-glucose and CREKA pentapeptide, composed of the amino acid residues Cys1, Arg2, Glu3, Lys4 and Ala5, using semiempirical molecular mechanics and quantum chemistry methods, parameterized for transition metal atoms. This complex is used for malignant tumorous disease therapies with the aim of delivering medicines to the affected tissue cells. Calculations were carried out by means of the computer program package HyperChem 8.03. The next stage of this research described magnetic particles that not only home to tumors, but also amplify their own homing [10,11]. The system is based on a magnetic aminodextran–CREKA peptide conjugate that can be used as an anti-tumor molecule [12]. Iron oxide nanoparticles can be coated with this aminodextran–CREKA peptide conjugate, thereby producing new binding sites for more particles [13,14]. These results show that the particle-bound peptide retains its binding with clotted plasma proteins [15].

2. Materials and methods

2.1 Materials

Pharmaceutical-grade dextran (PM 70, weight average molecular weight, 70,000) was obtained from Baku State University. All aqueous solutions were prepared using deionized water (NANO pure infinity), Barnstead/Thermolyne, Dubuque, IA, USA). Dimethylsulfoxide, ammonium persulfate and methanol were obtained from Aldrich Chemicals. All dextran conjugates were lyophilized and stored at -80°C. Dextran standards (stored at -80°C) were prepared by dissolution in deionized water followed by lyophilization. All other reagents were purchased from commercial suppliers and used as received.

2.2 Methods

2.2.1 Synthesis of allyldextran (PM70)
2.5g sodium hydroxide and 0.2g sodium borohydride was added to 10g PM70 dextran in 75 ml deionized water at 50°C and pH 11. The pH was maintained by dropwise addition of 2.5N NaOH and 2ml allyl bromide. After 3 h, the solution was neutralized with acetic acid (2.5mol/L) and placed in a refrigerator at 5°C for 2 h. After the top organic layer was decanted and 100 ml deionized water was added, the resulting solution was filtered (5μm) into an ultrafiltration cell and diafiltered (with a molecular weight cut off of 3000) with 10 exchange volumes of deionized water. The product, allyldextran, was then concentrated and lyophilized.

2.2.2 Synthesis of aminodextran conjugate

The allyldextran was reacted with 7.5g aminoalkyl thiol in 30ml dimethylsulfoxide to produce an aminodextran conjugate. This reaction was initiated with 0.1g ammonium persulfate and was performed under a nitrogen atmosphere. After 3 h, the reaction volume was doubled with deionized water, the solution was adjusted to pH 4 with sodium hydroxide (2.5 N), and the product was diluted with 140ml sodium acetate buffer (0.02 mol/L, pH 4). The product was then filtered (5μm) into an ultrafiltration cell and dialyzed with five exchange volumes of deionized water. After concentration, the aminodextran conjugate was lyophilized. A sample was then assayed for the average number of amino groups per dextran, which was defined as the amine density.

2.2.3 Synthesis of aminodextran-coated iron oxide nanoparticles

0.5g aminodextran conjugate and 35 mg $FeCl_3.6H_2O$ were dissolved in 4 ml H_2O under a flow of nitrogen for 1.5h. 14 mg $FeCl_2.4H_2O$ was added, followed by 100μL aqueous ammonia in two portions while the mixture was kept under nitrogen. The solution turned black and was heated to 80°C for 100min. After the mixture was cooled to room temperature, the ammonia was removed by flushing the solution with nitrogen for 10min. Freeze drying produced the desired particles (0.55mg), which are stable at 4°C for at least 1 year and were used for all further experiments. Titration of the resulting particles (18mg) with 0.1M HCl (0.85ml, 85μmol) and bromophenol blue in acetone/H_2O(1:1 ,10ml) resulted in 3.3 mmol COO^- g^{-1}. The particle size distribution experiments were carried out as described above.

2.2.4 The binding of aminodextran- coated iron oxide nanoparticles with CREKA peptide

We coupled fluorescein-labeled CREKA or fluorescein onto the surface of 50nm superparamagnetic, aminodextran-coated iron oxide (SPIO) nanoparticles. Such particles have been extensively characterized with regards to their chemistry, pharmacokinetics and toxicology and are used as MRI contrast agents. CREKA peptide (0.33mg, 0.23mmol) and magnetic nanoparticles (1.0mg, 3.3 mmolCOO^- , 20eq.) were dissolved in 500μl H_2O and the solution was shaken for 12h at room temperature. To purify the product an ultrafiltration device was used for centrifugation and after concentration the sample was washed with H_2O (3×2ml). Size-distribution experiments were carried out as described above.

3. Results and discussion

A detailed study of the spatial and electron structure of the iron (II) and iron (III) oxides and Fe_3O_4, preceded the investigation of the complex compound of Fe_3O_4 ($FeO \cdot Fe_2O_3$) with d-glucose and peptide CREKA. The resonance model of the Fe_3O_4 structure, including Fe=O and Fe_2O_3, was used, which is why there are results of the comparable analyses of the electron structures FeO, Fe_2O_3 and Fe_3O_4 the optimization of the valence geometry was carried out using the semiempirical method of molecular mechanics MM+. Figure 1a shows the calculation models of Fe_2O_3 and Fe_3O_4, and Figure 1b-1d show the generalized results of the geometrical parameter calculations and the calculations of the values of the partial charges on the atoms. The values of the contributions of various types of electron energy in the total energy after optimization of the electron structure of FeO, Fe_2O_3 and Fe_3O_4, as calculated using the semiempirical method of quantum chemistry PM3, are listed in Table 1.

In accordance with the results for the optimized structure of Fe_2O_3 the single bond length of Fe-O is 1.77 Å and the double bond length of Fe=O is 1.48Å. For the resonance structure of Fe_3O_4, its low energetic state corresponds to the structure where the bond length of Fe-O is 3.9 Å and the Fe=O bond length is 1.90 Å. The valence angle of Fe-O-Fe equaling 76.4° provides the most favorable balance of electrostatic interactions of oppositely charged atoms in Fe_2O_3. The angle in Fe_3O_4 is 109.5°, i.e. a little bit more than expected due to the Fe=O presence. Such an increase in valence angles is characteristic of the O--Fe=O bond. Whereas in Fe_2O_3 the value of this angle is 148.8^0, in Fe_3O_4 it makes ~180^0. This means that iron oxide $FeO \cdot Fe_2O_3$ has a strictly tetrahedral structure.
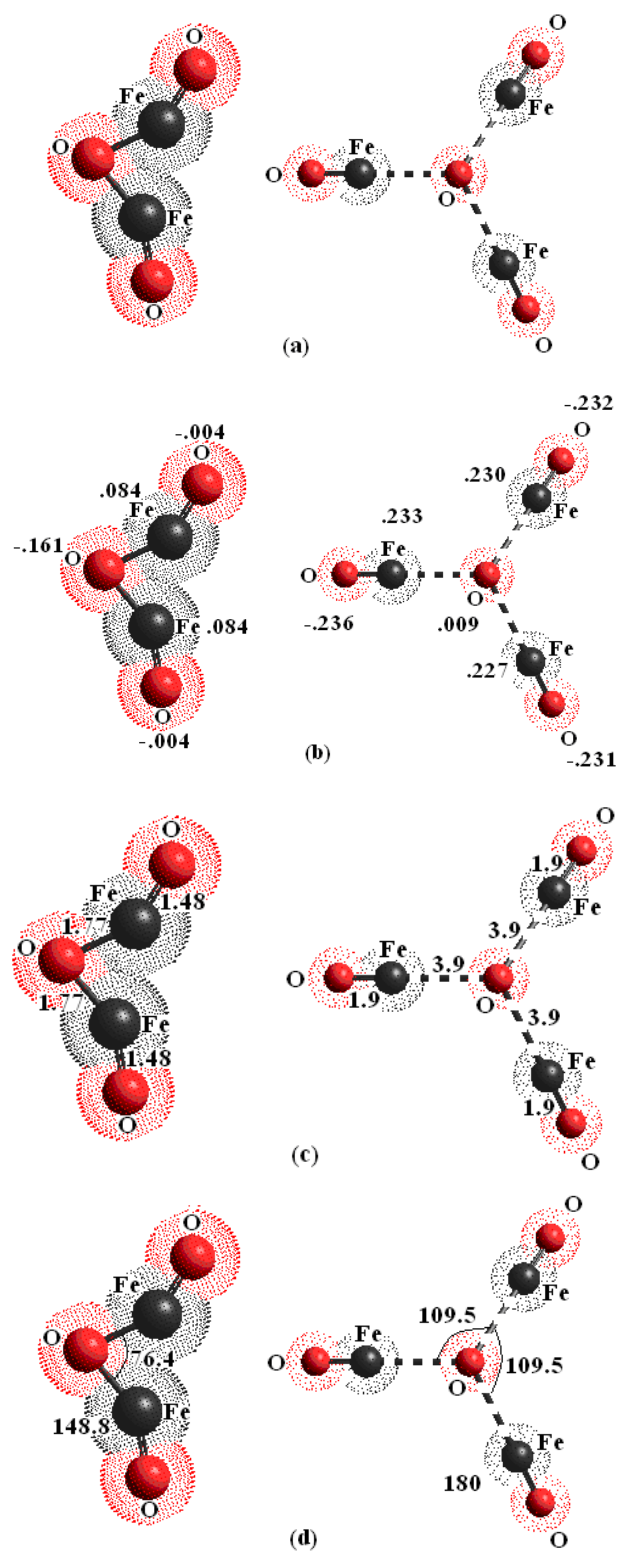
Fig. 1.Optimized structures of Fe₂O₃ and Fe₃O₄ using data from MM+ and PM3 methods:
(a) calculated model; (b) partial charges on atoms in electron charge units; (c) valence
bond lengths, Å; (d) valence angles, degrees

Table 1. Energy parameters and dipole moment iron oxide and Fe_3O_4 complexes with di-glucose and peptide CREKA according to PM3 method data

Compound (complex)	Total energy (kcal/mol)	Electron energy (kcal/mol)	Nuclease repulsion energy (kcal/mol)	Binding energy (kcal/mol)	Dipole momentum, D
FeO	-18686.68	-27040.04	8353.37	-13.95	1.61
Fe_2O_3	-44266.46	-97618.13	53351.67	-248.50	0.93
Fe_3O_4	-62846.49	-129565.76	66719.27	-155.81	2.63
Fe_3O_4 + di-glucose	-164526.47	-1258765.58	1094239.10	-4972.72	4.49
Fe_3O_4 + di-glucose+ CREKA-1	-334034.81	-4790443.65	4456408.85	-12498.93	47.45
Fe_3O_4 + di-glucose+ CREKA-2	-334141.39	-4769214.43	4435073.04	-12605.51	38.86
Fe_3O_4 + di-glucose+ CREKA-3	-334163.16	-4447260.03	4113096.87	-12627.28	32.84

Despite the differences in the total and electron energies of iron oxides, the repulsion energy of nucleases in $FeO \cdot Fe_2O_3$ is higher than in FeO and Fe_2O_3, at 58365.9 kcal/mol and 13367.60 kcal/mol, respectively. Consequently, the nuclease's repulsion energy in $FeO \cdot Fe_2O_3$ as a whole is 5014.23 kcal/mol higher than the sum of the repulsion energy of separated FeO and Fe_2O_3. By comparing the bonding energy parameters (Table 1) we can conclude that the difference in these values for Fe_2O_3 and Fe_3O_4 is 92.69 kcal/mol, i.e. the formation of Fe_2O_3 is preferred to the formation of $FeO \cdot Fe_2O_3$.

One important characteristic of molecules, which is crucial for their behavior in various force fields, is dipole momentum, which has an additive property. The optimized structures of FeO, Fe_2O_3 and Fe_3O_4 are characterized by dipole momentums equal to 1.61, 0.93 and 2.63, respectively (Table 1). These results indicate that the character of the molecular interactions of Fe_3O_4 with the medium, because of its high polarity, differs significantly from Fe_2O_3.

Comparison of the partial charges on the atoms of the compounds under investigation (Figure 1b) shows that the formation of Fe_3O_4 leads to a redistribution of electron density. As the result of this redistribution from the p-orbital of the central oxygen atom to the oxygen atom of FeO, a decrease in the negative charge value of the oxygen atoms (~ 0.233) was observed, and the iron atoms attained a formal positive charge of ~ 0.230 (Figure 1b).

In order to compare the reaction ability of the iron oxides, the values of the molecular orbital energies were analyzed and a comparative analysis of the energies of the highest occupied molecular orbital (HOMO) and the lowest unoccupied molecular orbital (LUMO) of Fe_2O_3 and Fe_3O_4 (Fig.2) was carried out.
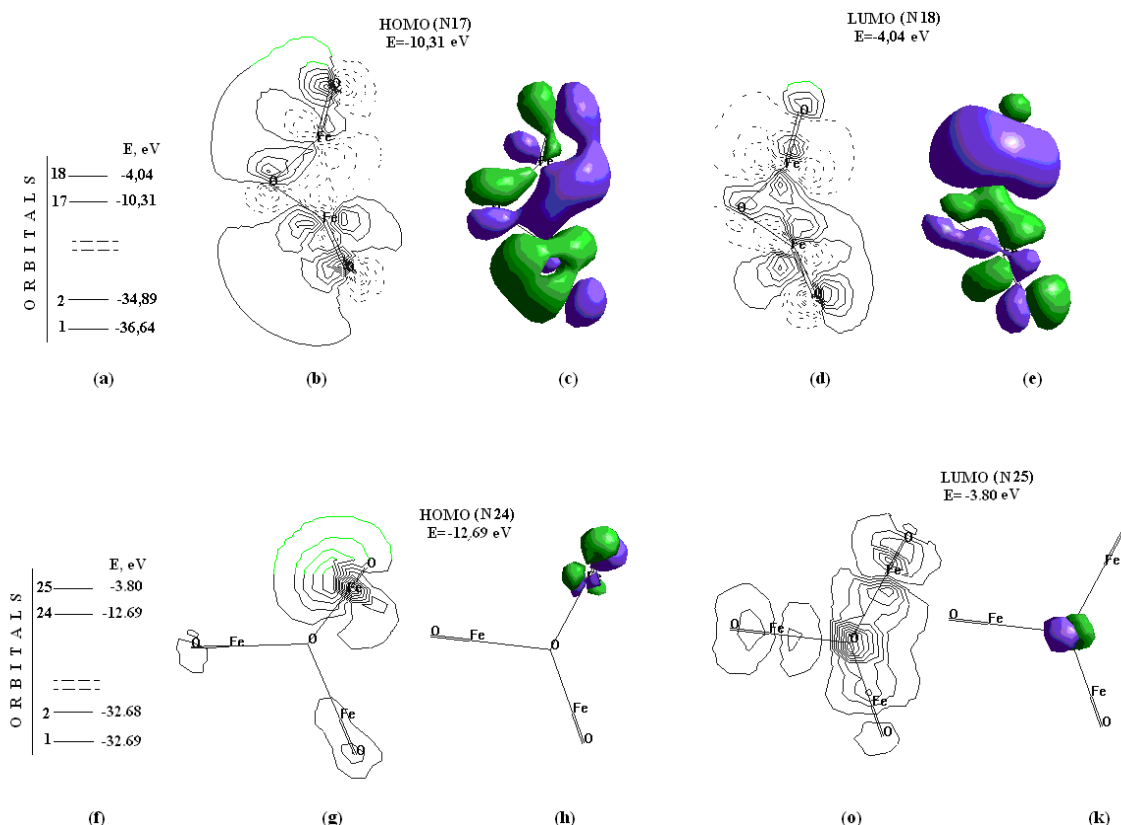
Fig. 2.Energy diagrams and two-dimensional and three-dimensional graphic images of the
highest occupied molecular orbital and lowest unoccupied molecular orbital
of Fe_2O_3 (a-e) and Fe_3O_4 (f-k).

In accordance with the approximation of valence electrons, the total number of electrons, considering the PM3 calculations, is equal to 34 and 48 respectively. In the ground state, electrons occupied 17 and 24 molecular orbitals. The ionization energies corresponding to the negative energy values for the Fe_2O_3 HOMO and Fe_3O_4 HOMO are equal to 10.31 and 12.69 eV, respectively. The energy difference of the first unoccupied orbital and HOMO is interpreted as the first energy of disturbance and equals 6.27 eV for Fe_2O_3 and 8.89 eV for Fe_3O_4. The lower the difference, the greater the electron affinity of the system.

On the basis of the results obtained and generalization of studies, a model of the complex including Fe_3O_4, di-glucose and CREKA has been constructed. First the spatial structure of complex Fe_3O_4 with bi-glucose was studied using semiempirical and molecular mechanic MM+ methods. The results are listed in Tables 1-3. These calculations (Table 2) show that the bond lengths of Fe-C (Fe_2-C_{33} and Fe_4-C_{10}) are 2.0Å, the bond lengths for Fe=O (Fe_2=O_1, Fe_6=O_7 and Fe_4=O_5) equal 1.73Å, and those for Fe-O are 1.89Å and 1.91 Å. From a comparison of the results obtained it follows that the Fe=O bond length in the complex with bi-glucose decreases from 1.9 to 1.73Å, while that for Fe-O decreases from 3.9Å to 1.9Å in comparison with Fe_3O_4. The valence angles that characterize the bonding part of Fe_3O_4 with bi-glucose change as follows: the O_3-Fe_2=O_1 and O_3-Fe_4=O_5 angles decrease to 118.83 and 117.76$^°$, respectively, while O_3-Fe_6=O_7 maintains a linear bond (~180$^°$) (Table 2). The angle Fe_2-O_3-Fe_4 decreases to 104.8$^°$. So complex formation with bi-glucose deforms the structure of Fe_3O_4, with the result being the redistribution of partial charges on the complex atom (Table 3). As per the calculations, the negative charge on the oxygen atom of iron oxide decreases O_1(Δ=0,167), O_5(Δ=0,164) and O_7(Δ=0,110) and the electron density on the iron atoms Fe_2, Fe_4 and Fe_6 increases. Consequently the partial charges on these atoms have negative values. The changes in the partial charges on the oxygen atoms of bi-glucose are negligible. So, complex formation of Fe_3O_4 with bi-glucose is accompanied by changes in geometry as well as electron and charge densities on the Fe and O atoms.

In the next stage of calculation, the structure of complex Fe_3O_4 with di-glucose and CREKA was studied. CREKA is a peptide composed of five amino acid residues, Cys1, Arg2, Glu3, Lys4 and Ala5, which is used for cancer treatments with nitrogen oxide and dextran (glucose polymer) to deliver the medication to tumorous cells. In the calculations three low energy conformations of CREKA were used, as calculated by the theoretical conformation analysis method and described in **[8, 9]**. They are labeled CREKA-1, CREKA-2 and CREKA-3 and differ by their dihedral angles values in the main and side chains of the amino acid residues (Figure 3).

Table 2- Parameters characterizing the complex structure of Fe_3O_4 with di-glucose by
MM+ methods

Spatial models of Fe_3O_4 with di-glucose

Bond	Length, Å
C_{33}-Fe_2	2.00
Fe_2=O_1	1.73
Fe_2-O_3	1.89
Fe_6 -O_3	1.91
Fe_6=O_7	1.73
Fe_4 -O_3	1.89
Fe_4-C_{10}	2.00
Fe_4=O_5	1.73
C_{10}-C_{11}	1.53
Valence angle	Value, degree
C_{33}-Fe_2-O_1	118.78
O_1-Fe_2-O_3	118.83
Fe_2-O_3-Fe_6	103.31
Fe_2-O_3-Fe_4	104.80
O_3-Fe_6=O_7	179.59
Fe_6-O_3-Fe_4	105.14
O_3-Fe_4=O_5	117.76
O_3-Fe_4-C_{10}	120.76
O_5=Fe_4-C_{10}	119.03
Torsion angle	Value, degree
O_{32}-C_{33}-Fe_2=O_3	-152.41
C_{33}-Fe_2-O_3-Fe_6	104.78
O_1=Fe_2-O_3-Fe_6	-52.84
O_1=Fe_2-O_3-Fe_4	-162.73
Fe_2-O_3-Fe_4=O_5	-68.57
Fe_2-O_3-Fe_6=O_7	-170.99
O_1=Fe_4-C_{10}-C_{11}	-123.36
O_7=Fe_6-O_3-Fe_4	-61.36
Fe_6-O_3-Fe_4=O_5	-177.12
O_3-Fe_4-C_{10}-C_{11}	74.81

Table 3. Charges (electron charge unit) on atoms Fe_3O_4 with di-glucose before and after optimization according to PM3 method data

Atom	Charge		Atom	Charge	
	before	after		before	after
Fe_2^*	0.227	-0.059	O_{13}	-0.279	-0.264
Fe_4	0.230	-0.060	O_{15}	-0.310	-0.343

Fe$_6$	0.233	-0.098	O$_{16}$	-0.306	-0.314
O$_1$	-0.231	-0.064	O$_{17}$	-0.317	-0.299
O$_5$	-0.232	-0.068	O$_{18}$	-0.290	-0.238
O$_3$	0.009	-0.002	C$_{29}$	0.024	0.038
O$_7$	-0.236	-0.126	C$_{30}$	0.051	0.051
C$_8$	0.020	0.058	C$_{31}$	0.011	0.035
C$_9$	0.055	0.030	C$_{32}$	0.018	0.020
C$_{10}$	0.008	0.055	C$_{33}$	0.193	0.133
C$_{11}$	0.018	-0.067	O$_{34}$	-0.284	-0.219
O$_{38}$	-0.301	-0.308	C$_{35}$	0.065	0.048
C$_{12}$	0.170	0.082	O$_{36}$	-0.314	-0.309
C$_{14}$	0.066	0.051	O$_{37}$	-0.317	-0.318

*Note: Numbering of atoms in coordination complex corresponds to diagram in Table 2

Calculations results are detailed in Figure 3 and Tables 1-4,5. As per Table 1, complex formation with bi-glucose accompanied a decrease in the total electron energy of up to 101 679.98 кcal/mol, and the addition of CREKA-1 in staggered conformation led to a decrease in the system energy of up to 233354.83 kcal/mol. The dipole momentum of the complex rapidly increased to 47.45D (in comparison with 4.49 for the Fe$_3$O$_4$complex with bi-glucose), which is indicative of the high reaction ability of the complex, containing as it does many charged groups. It should be noted that the optimization of complex geometry by the MM+ method does not bring about changes in the geometrical structure of the bonding area of Fe$_3$O$_4$with bi-glucose (Fig.3b-3d).
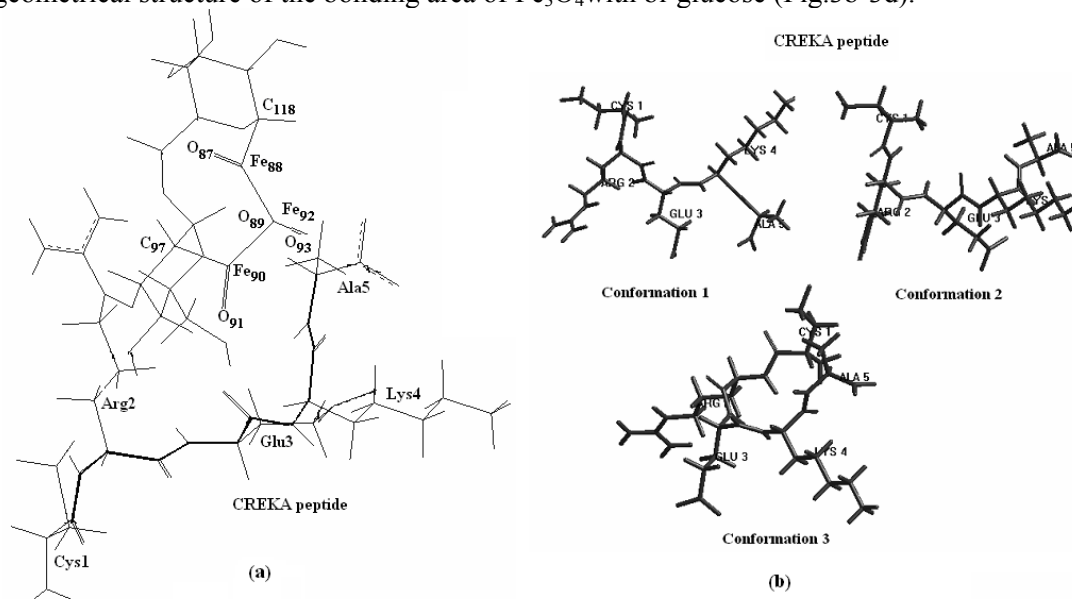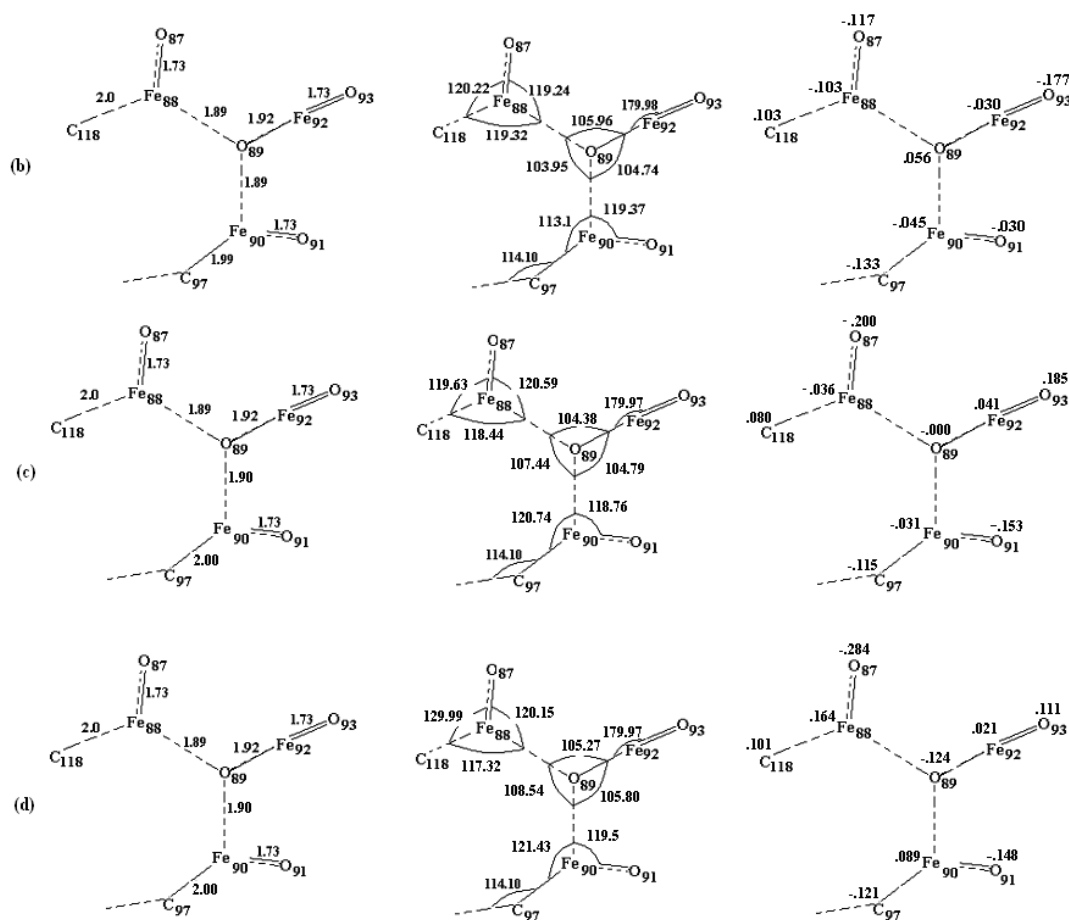
Fig. 3. Spatial model of complex composed of Fe₃O₄, di-glucose and CREKA (a);
conformations of CREKA molecule (b); bond length (Å), valence angles (degree) and
partial charges on atoms in various conformations of CREKA (b-d).

Valence angle values and bond length did not change significantly. It is interesting to compare of the partial charges on the complex atoms before and after binding with the peptide. The calculations show that an essential redistribution of electron density was observed for the Fe_{88} and O_{87} atoms. Shifting electron density from these atoms led to a decrease in the negative charge on Fe_{88} and O_{87}, by up to $\Delta=0.068$ and $\Delta=0.11$, respectively.

Analysis of the results (Table 1) reveals the energy preference of the complex containing CREKA-3 in conformation with amino acid residues Cys1 and Ala59 (Figure 3b). The distance between the C^{α}-atoms of Cys1 and Ala5 in this conformation is 6.1 Å, whereas in CREKA-1 and CREKA-2 this value is equal to 11.1 and 9.5 Å. Despite the energy difference between these conformations not exceeding 0.9 kcal/mol, in complexes of Fe_3O_4 with di-glucose this difference amounts to 128.35 kcal/mol. This complex is characterized by a compact structure in which Fe_3O_4 has a tetrahedral structure (Fig.3d).

$$Dextran-OH + Br-CH_2-CH=CH_2 \xrightarrow[NABH_4]{NaOH/50C} Dextran-O-CH_2-CH=CH_2 \quad (1)$$

$$Dextran-O-CH_2-CH=CH_2 \xrightarrow[\substack{Amonium\ Persulfate \\ DMSO/50\ C}]{C_6H_5CH_2NHCH_2\overset{\overset{SH}{|}}{CH}CH_2C_6H_5} Dextran-OCH_2CH_2CH_2 \quad (2)$$
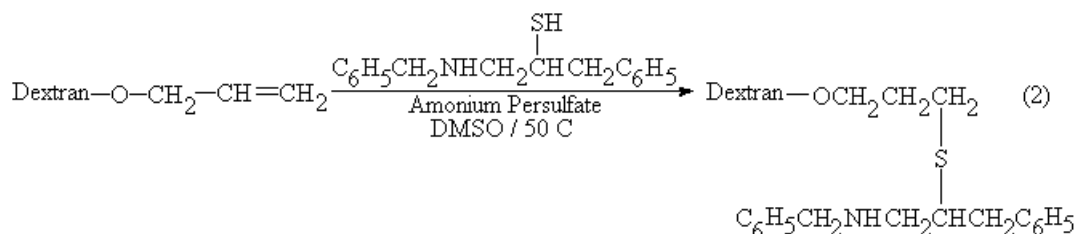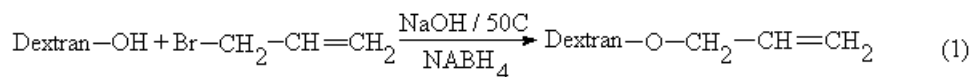
An important reason for choosing dextran as the molecular backbone is its practicality and availability. Therefore, active aminodextran molecules were synthesized in a two-step process (Fig.4).
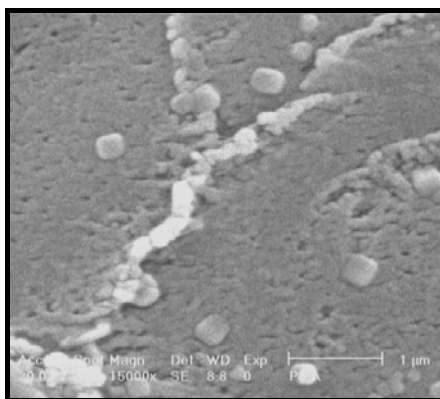
Fig. 4. Covalent attachment of amino groups to dextran hydroxyl groups in a two-step process, which prevents dextran cross-linking. DMSO, dimethyl sulfoxide.

Figure 5 shows scanning electron micrographs of aminodextran-coated iron oxide nanoparticles synthesized by chemical reaction. These nanoparticles are very sensitive to temperature. Scanning electron micrography images were obtained from a diluted solution of the nanocomposite particles.
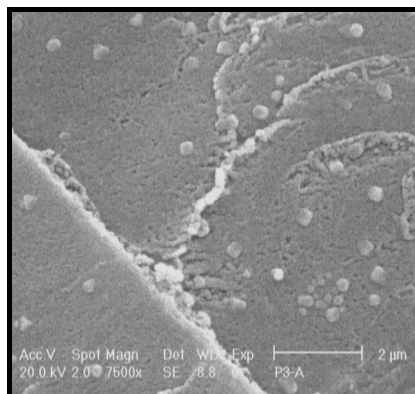
Fig. 5. Scanning electron micrographs of aminodextran- coated superparamagnetic iron oxide nanoparticles.

The ability of the aminodextran-coated iron oxide nanoparticles to form a complex with CREKA peptide depends on the nanoparticles, and the electrostatic interactions between the nanoparticles and the peptide. Therefore, it is possible to manipulate the incorporation process for CREKA peptide by an appropriate selection of the nanoparticles and the surface functionality. Figure 6 shows the X-ray diffraction (XRD) pattern of aminodextran-coated iron oxide nanoparticles.
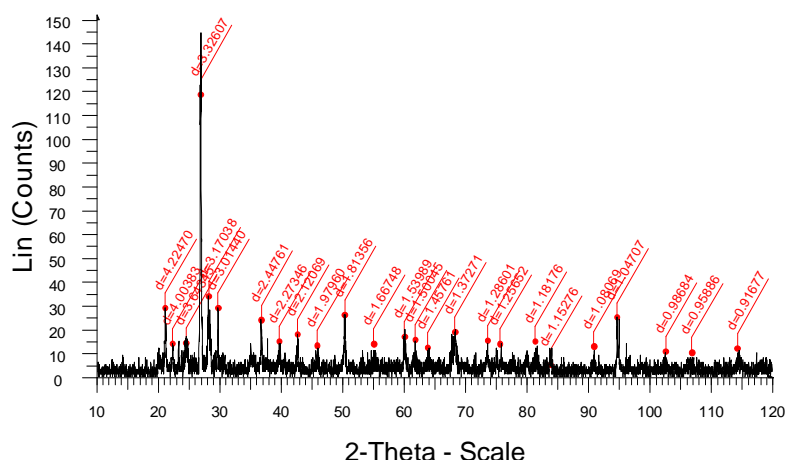
Fig. 6. X-ray diffraction of aminodextran-coated superparamagnetic iron oxide nanoparticles

XRD results for aminodextran–coated iron oxide nanoparticles show a strong peak at about $2\Theta = 26.46°$, which is a characteristic peak of aminodextran-coated iron oxide nanoparticles. Studies of XRD patterns of nanoparticles are scarce in the literature. Figure 7 shows the Fourier transform-infrared spectrum of aminodextran-coated iron oxide nanoparticles, where the % of transmittance is plotted as a function of wavenumber (cm^{-1}) . The wide peak around 3411 cm^{-1} is attributed to the O-H stretching vibrations of aminodextran. The peaks at 1523 and 1714cm^{-1} are attributed to the COO^{-} unsymmetrical and symmetrical stretching vibrations, respectively. The mean diameter of each conjugate was measured by dynamic light scattering (UPA-150; Honeywell-Microtrac, Clearwater, FL, USA). Each conjugate was assayed for 10 min at a concentration > 5mg/mL of 0.9% saline.
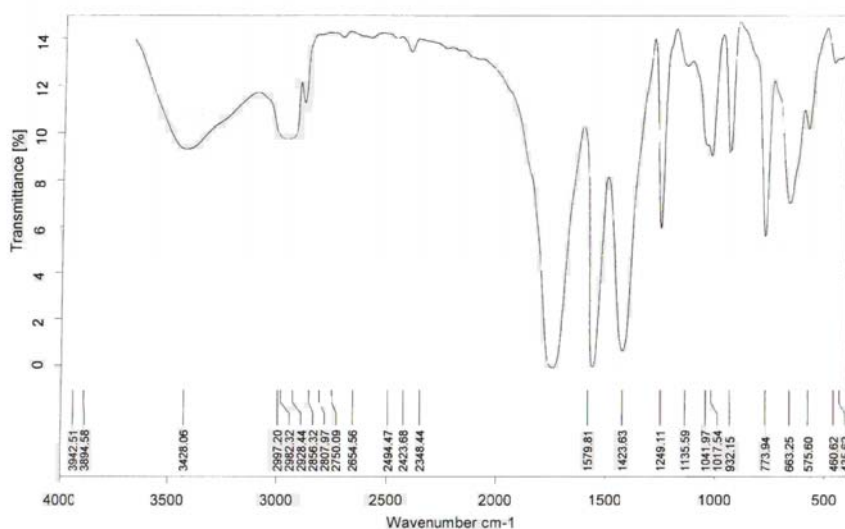
Fig. 7. Fourier transform-infrared spectrum of aminodextran-coated superparamagnetic iron oxide nanoparticles

The refractor index of each sample was assayed (Fisher Scientific, Santa Clara, CA, USA) and did not deviate from 0.9% saline. Latex particle standards of three different sizes gave weight-averaged diameters that were within 5% of their mean diameters (19 ± 1.5, 102 ± 3 and 993 ± 21 nm), which were calibrated by photon correlation spectroscopy or electron microscopy. The analyzer software did not assume a Gaussian size distribution. Mean molecular diameters with standard deviations were calculated from volume distribution data (Fig. 8).
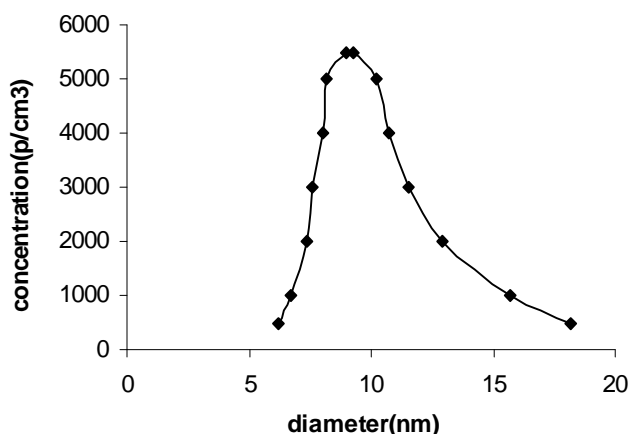
Fig. 8. Particle size distribution of aminodextran-coated superparamagnetic iron oxide /CREKA peptide conjugate

The average number of amino groups per dextran was measured in the following manner. The lyophilized dextran conjugate was dissolved in saline, and the amine concentration was measured by the trinitrobenzene sulfonate assay using hexylamine as a standard. The glucose concentration of the same sample was measured by the sulfuric acid method. The amino density was calculated by dividing the amine concentration by the glucose concentration and multiplication by the average number of glucose units per dextran.

4.Conclusions

Aminodextran–coated iron oxide nanoparticles are the first member of an important new class of agents based on a macromolecular backbone with a high density of sites for MRI reporters. This radiopharmaceutical is the first specifically designed as an anticancer drug carrier. Our long-term goal is to increase the pharmaceutical performance of the MRI technique. The result would be a wider dissemination of the technique, beyond academic centers, thus providing greater access for patients with cancer or melanoma.

References

[1] Petri-Fink, A.; Chastellain, M.; Juillerat-Jeanneret, L.; Ferrari, A. and Hofmann H. Biomaterials, **26**, 639 (2005).
[2] Koch, A.M.; Reynolds, F.; Merkle, H.P.; Weissleder, R. and Josephson, L. Biol. Chem. **6**, 337 (2005).
[3] Gould, P. Mater. Today, **7**(2), 36 (2004)
[4] Ruoslahti, E. Cancer Biol. Ther., **6**(2), 133 (2007).
[5] Simberg, D.; Duza, T.; Park, J.H.; Essler, M.; Pilch, J.; Zhang, L.; Derfus, A.M.; Yang, M.; Hoffman, R.M.; Bhatia, S.; Sailor, M.J. and Ruoslahti, E. PNAS, **104**(3), 932 (2007).

[6] Gamarra, L.F.; Brito, G.E.S.; Pontuschka, W.M.; Amaro, E.; Parma, A.H.C. and Goya, G.F. J. Magn. Magn. Mater., **289**, 439 (2005).

[7] Jain, T.K.; Morales, M.A.; Sahoo, S.K.; Leslie-Pelecky, D.L. and Labhasetwar, V. Mol. Pharmacol., **2**(3), 194 (2005).

[8] Abbasova, G.D.; Alieva, I.N.; Nabiyev, N.S.; Gojayev, N.M. and Ramazanov, M.A. J. Qafqaz Univ., **23**, 43 (2008).

[9] Gojayev, N.M.; Abbasova, G.D. and Alieva, I.N. J. Qafqaz Univ., **21**, 30-37.

[10] Shirakami, Y.; Mtsumura, Y.; Yamamichi, Y.; Kurami, M.; Ueda, N. and Hazue, M. Jpn. J. Nucl. Med., **24,** 475 (1987).

[11] Tomalia, D.A.; Baker, H. and Deward, J. Polymer J., **17**, 117 (1985).

[12] Porter, C.J.H. Crit. Rev. Ther. Drug Carrier Syst., **14**, 333 (1997).

[13] Nugent, J. and Jain, R.K. Cancer Res., **44**, 234 (1984).

[14] Thoren, L. "Dextran as a plasma volume substitute In: Jamieson G.A.; Greenwalt T.J.;"Blood substitutes and plasma expenders. New York , NY:Alan R. Liss; 265 (1978).

[15] Krejcarek, G.E. and Tucker, K.L., Biochem. Biophys. Res. Commun. **77**, 581 (1977).